Universities Council on Water Resources
Journal of Contemporary Water Research & Education
Issue 177, Pages 17-30, April 2023

Remote-Sensing Method for Monitoring Suspended-Sediment Concentration on the Middle-Mississippi and Lower-Missouri Rivers

Megan J. Martinez[1] and *Amanda L. Cox[1,2]

[1]*Civil Engineering, Saint Louis University, Saint Louis, Missouri*
[2]*WATER Institute, Saint Louis University, Saint Louis, Missouri*
**Corresponding Author*

Abstract: Sediment transport, erosion, and deposition are primary drivers of river geomorphic processes and ecological services. Suspended-sediment concentration (SSC) is an important parameter for evaluating these processes and is accordingly of significant interest to engineers, scientists, and water resource managers. The United States Geological Survey (USGS) previously operated nine daily SSC gauging stations along the Mississippi River, with operating dates ranging from 1974 to 2018. Currently, there are no USGS gauging stations reporting daily SSC values along the Mississippi River. For this study, regression models were developed to compute the SSC along the Middle-Mississippi River (MMR) and Lower-Missouri River (LMOR) using publicly and freely available Landsat imagery. Surface reflectance data from Landsat satellites were used with USGS-measured SSC to develop regression models for three different Landsat sensors (Landsat 8 OLI/TIRS, Landsat 7 ETM+, and Landsat 4-5 TM). Previous models published for predicting SSC in the MMR and LMOR from Landsat images have a linear-regression form and have provided invalid negative values when extrapolated outside of the dataset used for development. The objectives of this study were to develop reflectance-SSC regression models using a power-function form and demonstrate their extrapolation performance using multiple novel applications in the MMR basin. The reflectance-SSC regression models were applied to the following conditions: 1) mixing at the Mississippi and Missouri River confluence, 2) point-source pollution, and 3) SSC changes along the entire MMR reach for a range of discharges. The regression models were also used to develop sediment rating curves for the four largest tributaries of the MMR.

Keywords: *suspended-sediment concentration, remote sensing, water quality, Landsat, Mississippi River*

Suspended sediments play a significant role in fluvial environments. Sediment is constantly being transported and deposited in a water system, therefore, affecting channel geomorphology and ecological services. These characteristics impact channel navigability and ecological health, and should be monitored frequently. Methods for estimating suspended-sediment concentration (SSC) in fluvial environments have evolved over several decades, from in-situ measurements to multiple surrogate methods. Laser diffraction instruments, such as the Laser In-Situ Scattering and Transmissometry (LISST), can be submerged in water to directly measure laser diffraction, and therefore indirectly measure SSC (e.g., Gray and Gartner 2010; Felix et al. 2017; Dos Santos et al. 2018). Acoustic instruments such as an acoustic Doppler current profiler (ADCP) can measure acoustic backscatter in water, which has been correlated to SSC and can therefore be converted to provide a surrogate measurement of SSC (e.g., Landers 2012; Guerrero et al. 2017).

Remote sensing can also be used as a surrogate method to monitor water quality parameters such as SSC, chlorophyll, and temperature because changes in these parameters alter the energy spectra

Research Implications

- Provides a surrogate method to monitor suspended-sediment concentration (SSC) along the Middle-Mississippi River where SSC is not currently being monitored by the United States Geological Survey (USGS).
- Reduces the need for in-situ collection of SSC, therefore reducing labor and laboratory needs.
- Provides a method that can be used to develop similar models with available historical SSC and Landsat data.

of reflected solar and/or emitting thermal radiation from surface waters (Ritchie et al. 2003; Pereira et al. 2018; Peterson et al. 2018). Remote-sensing techniques of measuring SSC use surface reflectance measured by multispectral sensors in satellites or cameras. Surface reflectance can be correlated to SSC to provide an indirect measurement of SSC by creating surface reflectance-SSC models. Publicly available remote-sensing satellite imagery, such as Landsat, can be used to obtain cost-free data for monitoring spatial and temporal trends in SSC. Remote sensing as a surrogate method for monitoring SSC is particularly valuable for the Mississippi River as the United States Geological Survey (USGS) currently does not monitor SSC at any Mississippi River gauge stations, with 2018 being the last year of record.

Pereira et al. (2018) developed an empirical relationship between surface reflectance from Landsat satellites and SSC for the Middle-Mississippi River (MMR). Three empirical SSC models were developed for the following satellites: Landsat 4-5 Thematic Mapper (TM), Landsat 7 Enhanced Thematic Mapper Plus (ETM+), and Landsat 8 Operational Land Imager (OLI)/ Thermal Infrared Sensor (TIRS). The models were created to be used for further SSC studies along the MMR and its tributaries. However, when applied outside of the specific USGS gauge locations, several SSC values were predicted as negative values due to the linear form of the equations. The objectives of this study were to develop reflectance-SSC regression models using a power-function form and demonstrate their extrapolation performance using multiple novel applications in the MMR basin. The reflectance-SSC regression models were applied to the following conditions: 1) mixing at the Mississippi and Missouri River confluence, 2) point-source pollution, and 3) SSC changes along the entire MMR reach for a range of discharges. The regression models were also used to develop sediment rating curves for the four largest tributaries of the MMR.

Background

Several studies have investigated the relationship between Landsat surface reflectance and SSC (Richie et al. 1976; 1987; 1988; Topliss et al. 1990; Lathrop 1992; Mertes et al. 1993; Islam et al. 2001; Doxaran et al. 2003; Peterson et al. 2018). Ritchie et al. (1976) was one of the earliest studies to identify the optimum wavelength for quantitatively determining SSC of surface water from remote sensing. The study employed measured surface SSC data and spectrometer-measured reflected and incident solar radiation from six reservoirs in northern Mississippi, along with reflected solar radiation measurements from Landsat 1. The study found that the best spectral region to obtain a quantitative relationship between reflected solar radiation and SSC from surface water would be between 700 and 800 nm. Ritchie et al. (1987) developed multiple linear regression equations to estimate SSC in the surface water of Moon Lake from measured SSC data and reflectance measurements from Landsat Multispectral Scanner (MSS) data. Ritchie et al. (1988) tested the equations by comparing the predicted SSC with measured SSC from Moon Lake, an old oxbow lake off the Mississippi River in northwest Mississippi. The 1988 study found that when comparing single variable regressions with multiple variable linear regressions, the root mean squared error improved when adding up to three variables, but there was no improvement between three and four variables. The study also determined that the best equations for estimating SSC were based on Landsat MSS Near-Infrared (NIR) band (700 to 800 nm), but because of the linear form, all equations appeared to underestimate SSC at high concentrations.

Lathrop (1992) studied the relationship between Landsat 4-5 TM reflectance and measured

SSC from the Green Bay-Lake Michigan and Yellowstone Lake in Wyoming. The study found that the reflectance in the longer red and NIR wavelengths increased faster than in the shorter blue and green wavelengths. Lathrop (1992) also showed that the relationship between individual band reflectance and the ratio band combinations is nonlinear, approximating the general form of a power model. Long and Pavelsky (2013) compared 31 published empirical equations using a field dataset containing 147 observations of SSC and in-situ spectral reflectance to identify an appropriate reflectance-SSC model. Success of the reflectance-SSC models was contingent on the equation meeting the following criteria: 1) use of the NIR band in combination with at least one visible band, 2) development based on SSC like those in the observed region, and 3) use of a non-linear equation form (Long and Pavelsky 2013).

Regression Model Development

Data and Study Area

Landsat Satellite Data. The Landsat project is part of the Remote Sensing Missions component of the USGS Land Remote Sensing (LRS) Program. Landsat satellites have been collecting remote-sensing data for over 40 years with a temporal resolution of 16 days for each satellite. Landsat has the longest temporal record of moderate resolution multispectral data of the Earth's surface on a global basis. Data from Landsat 4-5 TM, 7 ETM+, and 8 OLI/TIRS were used for this study.

Landsat 4-5 TM has data available from July 1982 until January 2013, Landsat 7 ETM+ has data from April 1999 to April 2022, and Landsat 8 OLI/TIRS has data available from February 2013 until the present. Landsat 4-5 TM collection includes six, 30-m resolution spectral bands ranging from visible green to NIR wavelengths, two shortwave infrared (SWIR) bands, and a 120-m resolution thermal infrared (IR) band. Landsat 7 ETM+ collection includes 30-m resolution visible, NIR and SWIR bands, a 60-m resolution thermal band, and a 15-m panchromatic band. Landsat 8 OLI/TIRS collection includes 30-m resolution visible, NIR and SWIR bands, a 15-m resolution panchromatic band, two thermal bands, a coastal-aerosol band, and a band for cirrus cloud detection.

In 2016, the USGS started reorganizing the Landsat archive into a formal tiered data collection structure. Tier 1 (T1) data have the highest available geometric and radiometric quality. They include precision terrain processing and have been inter-calibrated across the Landsat sensors. The equations from Pereira et al. (2018) were developed using Landsat data before the application of this collection structure, and utilized all the images without the tier quality indicator. For this study, only T1 data were used for developing the regression models.

USGS Water Quality Gauge Stations. The USGS operates several gauge stations throughout the MMR, but only a small fraction of the stations has historical SSC data. This study used daily SSC data from four USGS gauge stations: i) Thebes, Illinois on the Mississippi River; ii) Hermann, Missouri on the Missouri River; iii) Chester, Illinois on the Mississippi River; and iv) St. Charles, Missouri on the Missouri River (Figure 1). These data were accessed through the USGS National Water Information System (NWIS) Web Interface. The beginning and end dates of the periods of record used in this study at each gage site are listed in Table 1. The Thebes, Hermann, Chester, and St. Charles gauging stations began their periods of record in 1982, 2009, 1982, and 2005, respectively. The period of record ended in 2017 for Thebes and Chester, and in 2008 for St. Charles. The Hermann station, located on the Missouri River, is currently continuing to provide daily SSC data.

Methods

Landsat Data Processing. Landsat T1 band surface reflectance values for blue, red, green, and NIR bands were used as independent variables in the regression model development. Surface reflectance values were obtained from delineated sampling areas at the four USGS gauge station locations. The rectangular sampling areas were 100 m wide by 330 m long. In MATLAB, each Landsat image was imported using an original MATLAB code, and the sampling area was delineated. The mean surface reflectance and standard deviation were calculated for each reflectance band of interest (green, blue, red, and NIR) within the sampling area.

The following chronological filters were used on each Landsat image to generate the final Landsat surface reflectance dataset: collection tier filter, pixel quality filter, blue band mean surface reflectance filter (removes images with cirrus cloud coverage in the sample area), and surface reflectance standard deviation filter (removes images with vessels in the sampling area). The collection tier filter only allows T1 Landsat images to be used, and the pixel quality filter only allows pixels to be used if they are defined as "low cloud confidence". The blue-band mean surface reflectance filter was then used to identify and remove images with values higher than 4.5% for Landsat 8 OLI/TIRS images, and 6.5% for Landsat 7 ETM+ and Landsat 4-5 TM images.

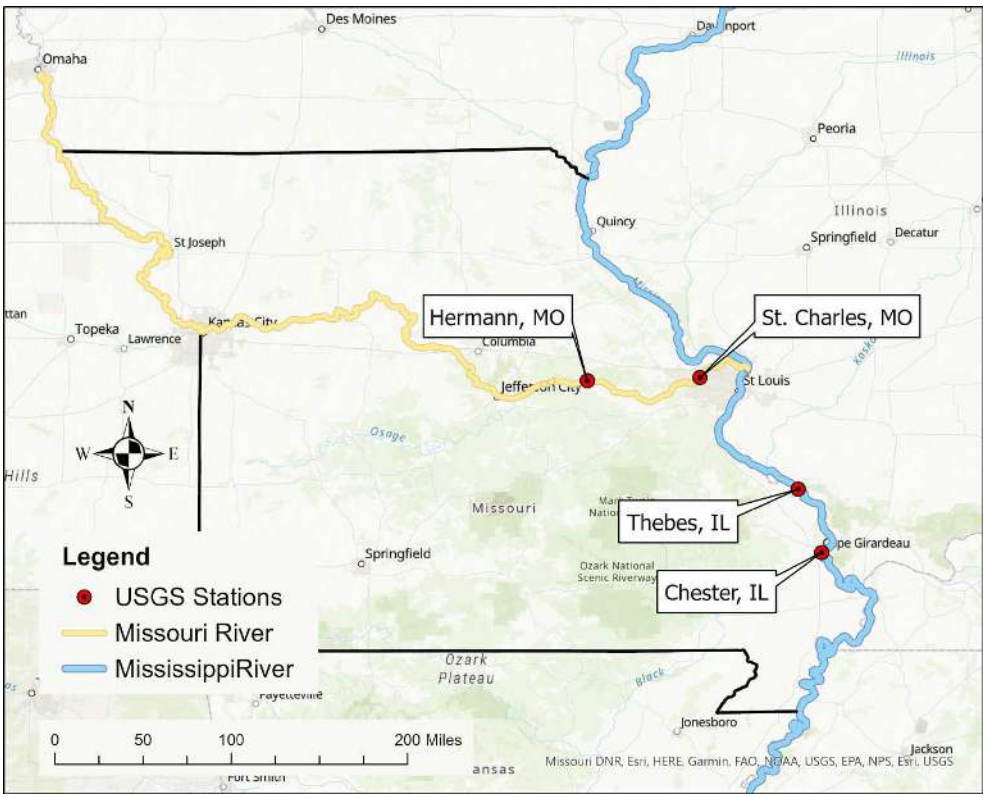

Figure 1. USGS gauge station locations used in regression equation analysis.

Table 1. Summary of development group and validation group USGS water quality gauge stations used in the development of the regression model.

Group	USGS Gauge Station (Location - Gauge No.)	Begin Date	End Date	------- No. of Data Points -------		
				L8 OLI/TIRS	L7 ETM+	L4-5 TM
Development	Thebes, IL – 07022000 Mississippi River	1982	2017	15	122	151
Development	Hermann, MO – 06934500 Missouri River	2009	2017	22	41	17
Validation	Chester, IL – 07020500 Mississippi River	1982	n/a	21	95	70
Validation	St. Charles, MO – 06935965 Missouri River	2005	2008	0	14	13

Lastly, the surface reflectance standard derivation filter identified and removed images with a surface reflectance standard deviation for any band greater than 0.5%. Details of the development of the blue-band and standard deviation filter methods are provided in Pereira et al. (2018). These steps ensured a high quality of Landsat data used in the development of the models.

Composite Dataset. The complete final dataset consisted of USGS daily SSC data and mean surface reflectance for the blue, green, red, and NIR bands. Each Landsat image product is representative of one date, and therefore dates in the Landsat dataset had to be matched to a date with a USGS SSC daily record. Each data point in the composite dataset is, therefore, representative of one date where there is both Landsat data and USGS data available. The temporal range of each final dataset varied among Landsat sensors. A summary of the Landsat data is provided in Table 1. Landsat 4-5 TM used data from almost 29 years, with a date range of January 1983 to November 2011; Landsat 7 ETM+ used data from nearly 18 years, with a date range of August 1999 to July 2017; and Landsat 8 OLI/TIRS used data from almost four and a half years, with a date range of March 2013 to July 2017.

Regression Analysis. The following power equation form was used for developing the regression model:

$$SSC = \alpha X_1^{\beta 1} X_2^{\beta 2} X_3^{\beta 3} + \varepsilon \quad (1)$$

where SSC is predicted in mgL^{-1}, α is the regression coefficient, ε is a constant term, X_1, X_2, and X_3 are band reflectance ratios Blue:NIR, Green:NIR, and Red:NIR, respectively, and β_1, β_2, and β_3 are exponents of band reflectance ratios X_1, X_2, and X_3, respectively. The least-squares fitting method was used to determine the optimal exponents and coefficients for Equation (1) for each of the regressions (i.e., Landsat 4/5 TM, Landsat 7 ETM+, and Landsat 8 OLI/TIRS).

For regression model development, the dataset was split into a development group (Thebes and Hermann) and a validation group (Chester and St. Charles). Regression coefficients and exponents were calibrated using data from the development group, and data from the validation group were used to independently assess the performance of the regression model. Splitting the development and validation datasets by location provided the best ability to assess the regional transferability of the regression models.

The St. Charles gauge station was not used in the validation group for Landsat 8 OLI/TIRS regression analysis because the gauge stopped reporting SSC data in 2008, before Landsat 8 OLI/TIRS was launched. Pereira et al. (2018) also included the St. Joseph gauge station in the validation group; however, when performing regression analyses, data from the St. Joseph station did not fit the regression trends for all Landsat sensors. Although St. Joseph is also on the Missouri River, the station is located 563 river kilometers upstream of the Herman station on the Missouri River. This finding reflects the significance of spatial transferability on reflectance-SSC empirical relationships.

Results and Discussion

A comparison between surface reflectance in visible and NIR Landsat bands and USGS daily SSC data showed that surface reflectance increases with increasing measured SSC. The peak surface reflectance within Landsat 8 OLI/TIRS visible and NIR bands alternated between the green (0.533 to 0.590 µm) and red (0.636 to 0.673 µm) bands for SSC values less than 155 mgL^{-1}. For SSC values greater than 155 mgL^{-1}, the peak reflectance switched to the red band. Landsat 7 ETM+ and Landsat 4-5 TM surface reflectance had peak reflectance in the green band (0.52 to 0.60 µm) when the SSC value was less than 140 mgL^{-1}. Peak reflectance alternated between green and red (0.63 to 0.69 µm) bands when the SSC value was between 140 to 160 mgL^{-1}, and at SSC values greater than 160 mgL^{-1} the peak was sustained in the red band. Pereira et al. (2018) show an example of the surface reflectance spectrum for Landsat 7 ETM+ and Landsat 4-5 TM.

Spectral sensitivity in Landsat bands was consistent when comparing Mississippi and Missouri River stations. The Mississippi River at Hermann and the Missouri River at Thebes showed similar spectral shapes (Figure 2). Lower SSC demonstrated peak reflectance in the green and red bands for both Hermann and Thebes. Concentrations higher than 155 mgL^{-1} had peak reflectance in the red band consistently for both

Hermann and Thebes, as well. This finding shows consistency in spectral sensitivity with spatial variability.

The calibrated reflectance-SSC regression models are provided in Table 2, and comparisons of observed versus predicted SSC values for the development and validation groups are shown in Figures 3 and 4, respectively. The regression exponents for all three models indicate the highest correlations with the green to NIR band ratio. The red to NIR ratio also had a relatively large exponent compared to the exponents for the blue to NIR band ratios. A summary of the statistical performance of the three regression models is shown in Table 3. For each regression model, the coefficient of determination (R^2) and the root mean square error (RMSE) statistics are reported for the development group, validation group, and the entire dataset.

For Landsat 4-5 TM, the development and validation groups included 168 and 83 records, respectively. The Landsat 4-5 TM regression model had development and validation R^2 values of 0.70 and 0.75, respectively. The increase in R^2 between the development and validation groups indicates that the regression model is not overfitting the development data and that the model is regionally transferable.

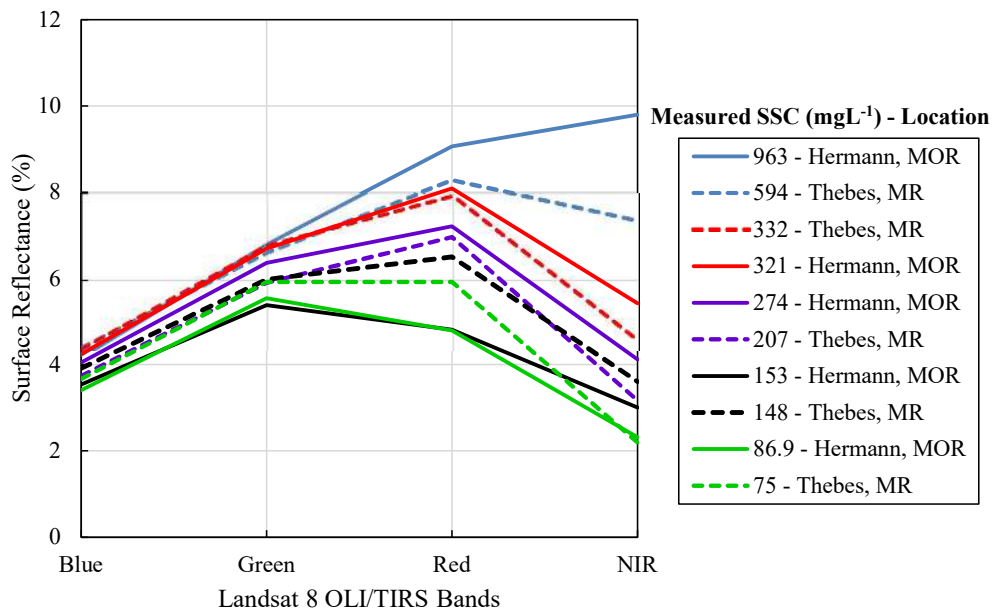

Figure 2. Comparison of spectral sensitivity for Mississippi and Missouri Rivers at similar SSC values.

Table 2. Reflectance-SSC empirical relationships for Landsat 8 OLI/TIRS, 7 ETM+, and 4-5 TM.

Landsat Sensor	Reflectance-SSC Empirical Relationship
8 OLI/TIRS	$SSC\ (\mathrm{mgL^{-1}}) = 159.9 \left(\frac{b2}{b5}\right)^{-0.1337} \left(\frac{b3}{b5}\right)^{-5.182} \left(\frac{b4}{b5}\right)^{3.663} + 87.67$
7 ETM+	$SSC\ (\mathrm{mgL^{-1}}) = 111.3 \left(\frac{b1}{b4}\right)^{-0.2684} \left(\frac{b2}{b4}\right)^{-6.033} \left(\frac{b3}{b4}\right)^{5.031} + 63.84$
4-5 TM	$SSC\ (\mathrm{mgL^{-1}}) = 74.80 \left(\frac{b1}{b4}\right)^{-1.387} \left(\frac{b2}{b4}\right)^{-4.639} \left(\frac{b3}{b4}\right)^{4.227} + 80.68$

Note. For Landsat 8 OLI/TIRS, *b*2, *b*3, *b*4, and *b*5 are blue, green, red, and NIR band surface reflectance, respectively; and for Landsat 7 ETM+ and 4-5 TM, *b*1, *b*2, *b*3, and *b*4 are blue, green, red, and NIR band surface reflectance, respectively.

For Landsat 7 ETM+, the development and validation groups included 163 and 109 records, respectively. The Landsat 7 ETM+ regression model had development and validation R^2 values of 0.74 and 0.71, respectively. Similar to the Landsat 4-5 TM regression, the minimal difference between the development and validation group R^2 values indicates a lack of model overfitting and regional transferability.

For Landsat 8 OLI/TIRS, the development and validation groups included 37 and 21 records, respectively. The Landsat 8 OLI/TIRS dataset included a total of 58 records which is 23% and 21% of the number of Landsat 4-5 TM and Landsat 7 ETM+ records, respectively. The Landsat 8 OLI/TIRS regression model had development and validation R^2 values of 0.95 and 0.72, respectively.

Table 3. Summary of R^2 and RMSE for the Reflectance-SSC regression models.

	8 OLI SSC	7 ETM+ SSC	4-5 TM SSC
Range (mgL^{-1})	49-963	41-961	44-863
No. of Samples	58	272	251
R^2_{Dev}	0.95	0.74	0.70
R^2_{Val}	0.72	0.71	0.75
R^2_{All}	0.87	0.73	0.72
$RMSE_{Dev}$	37	82	85
$RMSE_{Val}$	89	85	80
$RMSE_{All}$	61	83	83

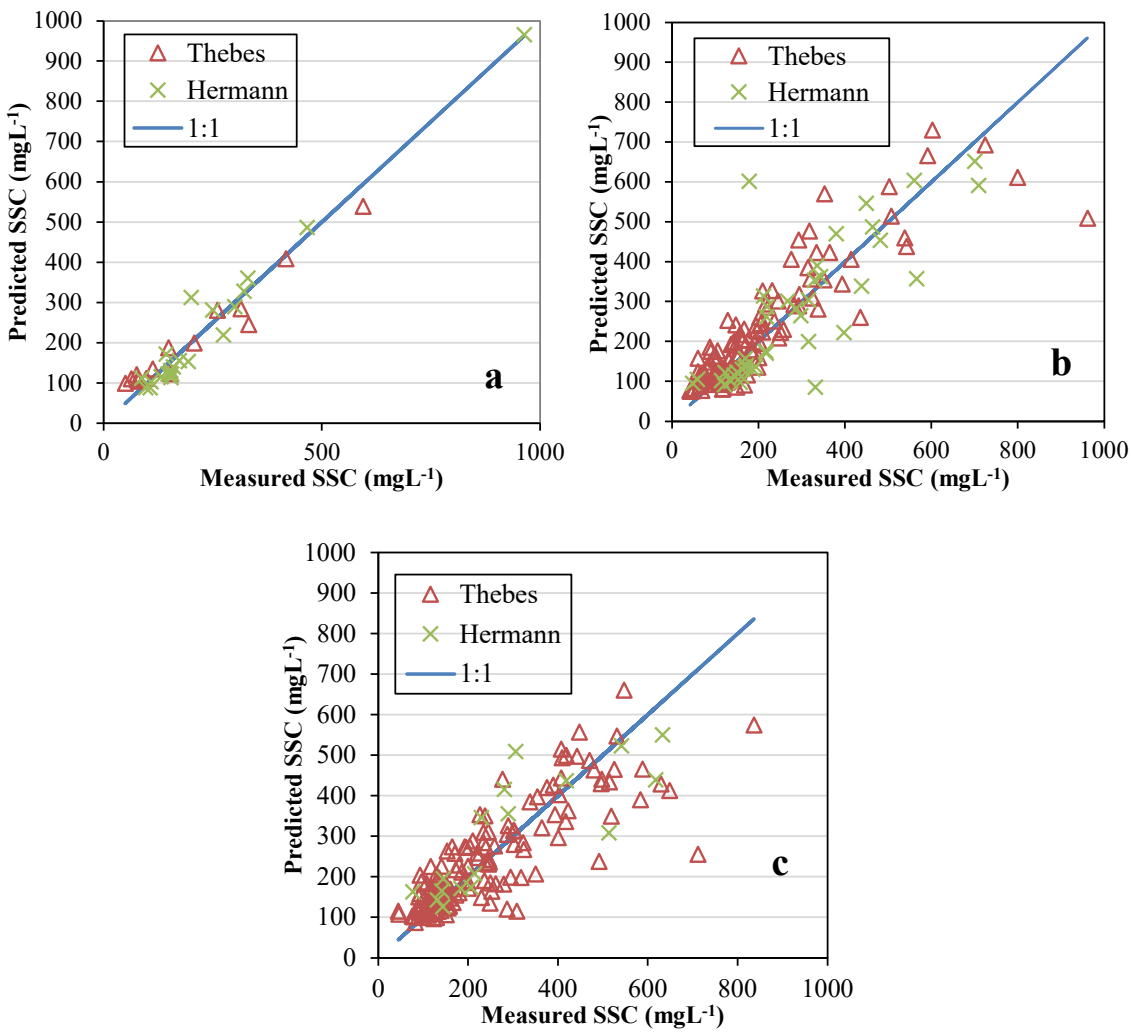

Figure 3. Development group relationship between predicted SSC and observed SSC for (a) Landsat 8 OLI/TIRS, (b) Landsat 7 ETM+, and (c) Landsat 4-5 TM.

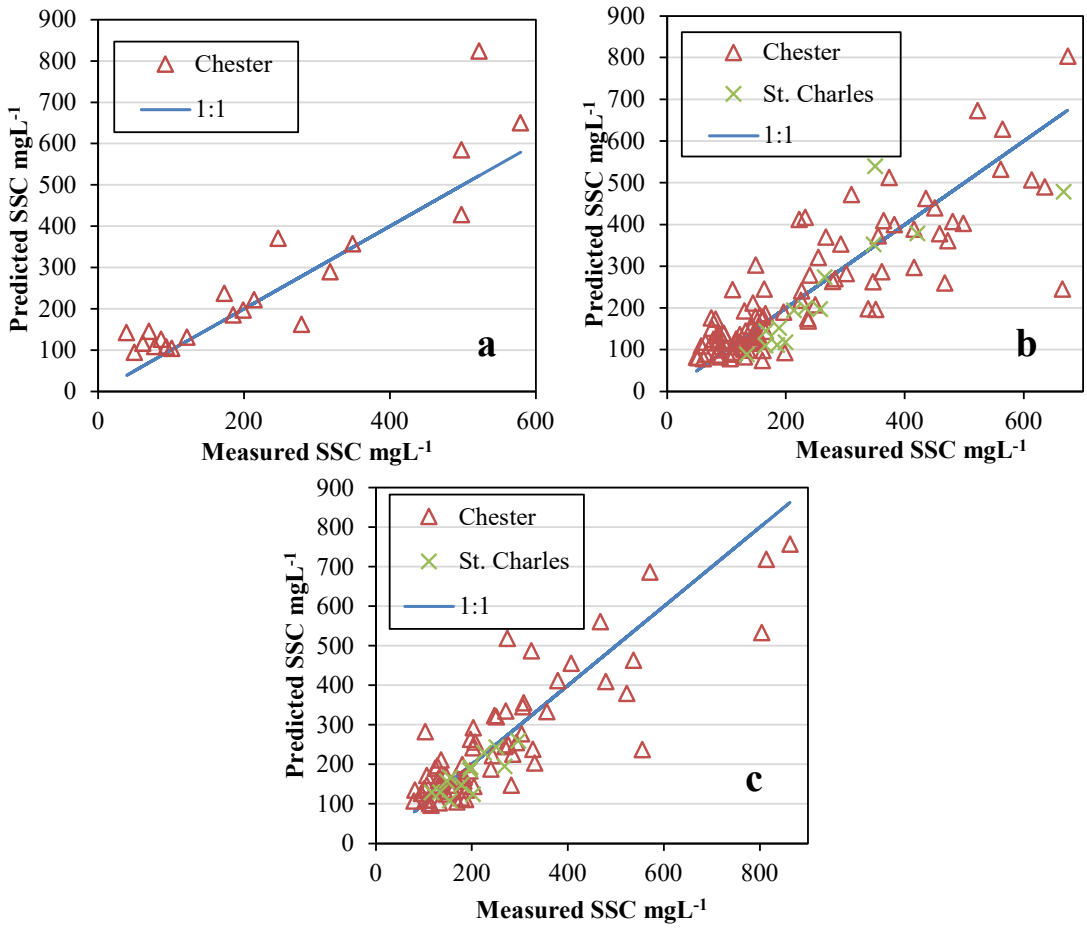

Figure 4. Validation group relationship between predicted SSC and observed SSC for (a) Landsat 8 OLI/TIRS, (b) Landsat 7 ETM+, and (c) Landsat 4-5 TM.

The high development R^2 value is a strong indication of the potential for the Landsat 8 OLI/TIRS sensor to predict SSC; however, the notably lower validation R^2 value suggests that the model is overfitting and that more records are needed to develop a robust regression model.

The power-regression form of the reflectance-SSC model has several advantages over the model provided by Pereira et al. (2018):

- Power-regression model does not allow for any negative estimated SSC values which were observed during the application of the Pereira et al. (2018) model;
- Approximately two additional years of period of record were used in the combined development and validation dataset;
- The revised filtering methodology is consistent with the updated Landsat product formats (i.e., Tier quality classifications); and
- R^2 values (0.62 to 0.72 for the validation group) were notably improved for the Landsat 8 model (negligible differences in Landsat 4/5 and Landsat 7 models) likely due to the increased number of data points used in the model development.

Reflectance-SSC Regression Applications

Confluence Mixing

The Landsat 8 OLI/TIRS regression model was applied at the confluence of the Mississippi and Missouri Rivers to analyze the difference in SSC between the two rivers and evaluate the downstream mixing length. The Landsat real-color image of the Mississippi–Missouri River confluence from September 12, 2016, shown in Figure 5, illustrates a visible color difference between the flow from the Mississippi River and

the Missouri River. On this date, discharges in the Mississippi River and Missouri River were 9,940 cubic meters per second (cms) and 4,191 cms, respectively, with corresponding exceedance probabilities of 15% and 25%, respectively. The SSC distribution computed from the Landsat 8 OLI/TIRS regression model is also shown in Figure 5. The computed SSC values for the Mississippi River and Missouri River were 700 mgL^{-1} and 200 mgL^{-1}, respectively. For this image, the computed and visible mixing divide extended approximately 161 river kilometers downstream.

Point-Source Pollution

Along the MMR, areas of abnormally high SSC can be identified and quantified using reflectance-SSC regression models. Figure 6 shows an area of high SSC at the same location on four different dates between 2014 and 2017. The SSC data in Figure 6 were developed using the Landsat 8 OLI/TIRS regression model. Figure 6-f shows the same point in 2013, but the area has no noticeably higher concentration. The discharge on the 2013 date was 1087 cms (observed at St. Louis Gage Station 0701000), which was significantly lower than the discharges on the other dates, which ranged from 5,692 cms to 7,108 cms. This reduced flow rate is likely the cause of the lack of increased SSC in the area of concern.

Using the reflectance-SSC regression models, an automated algorithm could be developed to process the entire reach of the MMR and quantify local regions of increased SSC. Applying this automated method with images from several dates could then be used to identify zones with consistently higher SSC values. This application could be a powerful tool for environmentalists or government agencies to ensure that regulations are being properly followed.

Analysis across Large River Reaches

The three regression models were used to investigate profile distributions of SSC along the main channel of the Mississippi River. Landsat-predicted SSC values were obtained from 33,000-m^2 sampling areas along the MMR every 16 river

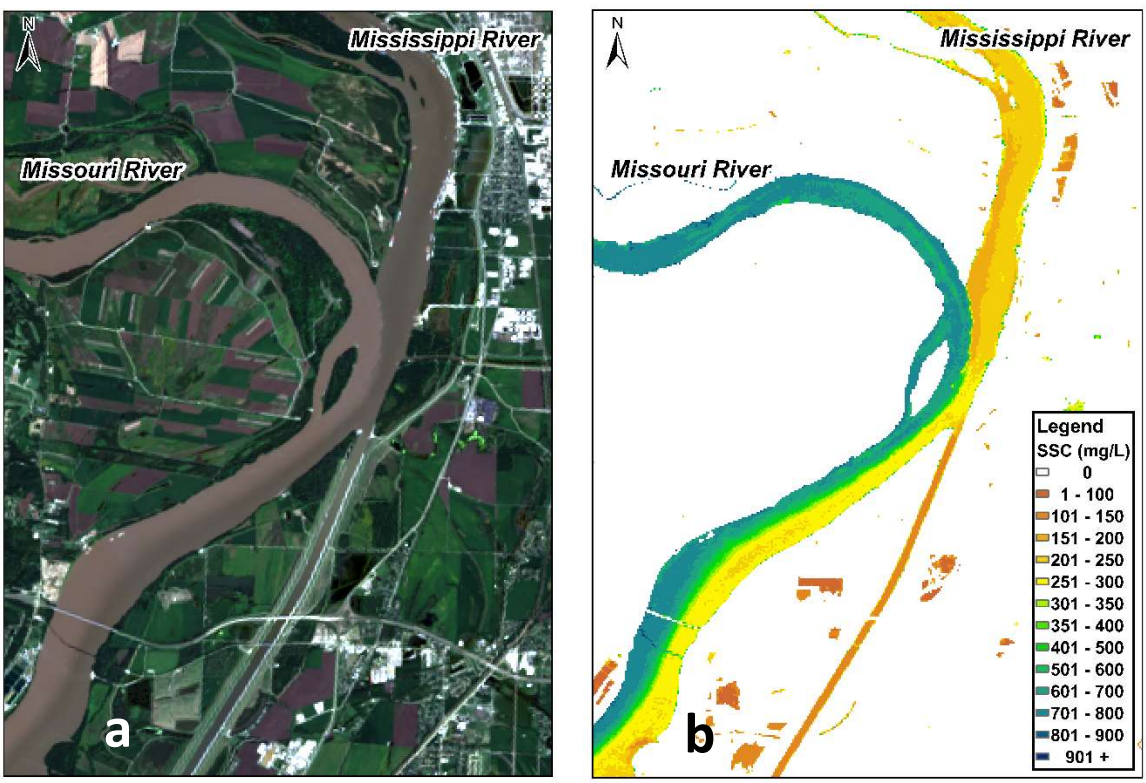

Figure 5. Mississippi–Missouri River confluence from Landsat 8 Surface Reflectance Image on September 12, 2016 (a) Landsat Real Color Image and (b) Landsat-Predicted SSC Image.

kilometers for the following dates: September 29, 1993 (Landsat 4-5 TM); September 4, 2010 (Landsat 7 ETM+); and November 13, 2015 (Landsat 8 OLI/TIRS). These dates were selected to include a low, medium, and high discharge condition. The Mississippi River discharges on these dates, extracted from the St. Louis USGS Gage (07010000), were 19,539, 8,948, and 3,766 cms, respectively, with corresponding exceedance probabilities of 1%, 19%, and 72%, respectively. The Missouri River discharges on these dates were 13,168, 3,710, and 1,487 cms, respectively, with corresponding exceedance probabilities of 0.12%, 21%, and 67%, respectively.

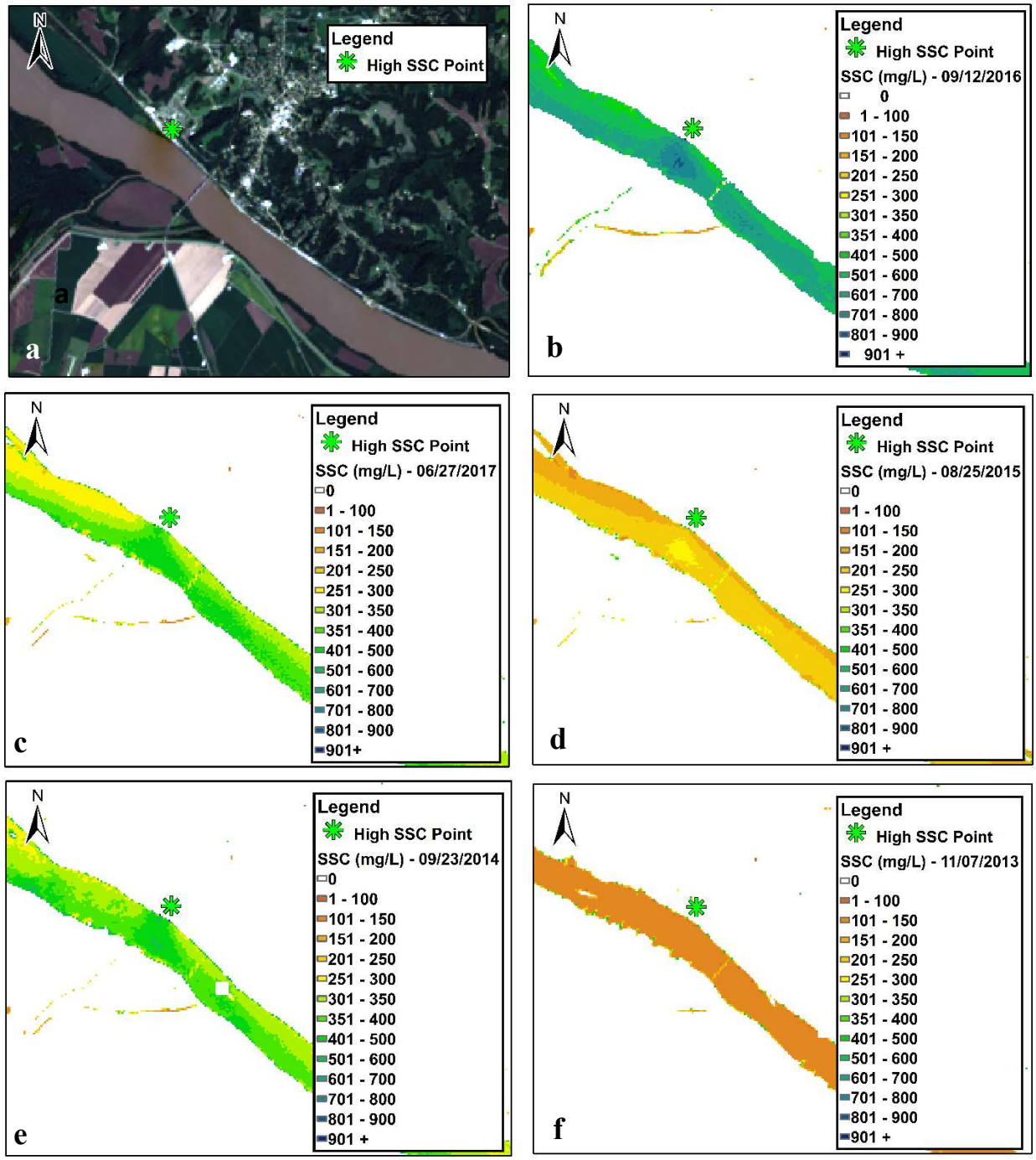

Figure 6. High SSC point along the MMR showed on (a) Landsat Real Color Image - 09/12/2016, Landsat-Predicted SSC Image, (b) 09/12/2016, (c) 06/27/2017, (d) 08/25/2015, (e) 09/23/2014, and (f) 11/07/2013.

Computed SSC values as a function of river kilometer are shown in Figure 7. The results show that SSC values generally increased with increasing downstream distance and increased with increasing water discharges. The September 29, 1993 data show a drastic spike downstream of the Missouri River confluence. This date occurred during the great Mississippi River and Missouri River flood, which lasted from April to October 1993, and had disproportionally high-water discharges in the Missouri River relative to the Mississippi River.

Sediment Rating Curves

The final demonstrated application of the reflectance-SSC regression models is the development of sediment rating curves for the following MMR tributaries: the Missouri, Meramec, Kaskaskia, and Big Muddy Rivers. Due to the 30-m resolution of Landsat imagery, only the tributaries that had a median channel width of 30 m or greater were used in this application. SSC data for each tributary were obtained using all available Landsat 4-5 TM, Landsat 7 TM+, and Landsat 8 OLI/TIRS, the image filtering techniques described in the Methods Section, and the reflectance-SSC regression models. All sampling areas were 33,000 m^2 rectangular areas located immediately upstream of each confluence. The median channel width of each tributary varied; therefore, sample area dimensions for each tributary were as follows: 100 m wide by 330 m long for the Missouri River, 60 m wide by 550 m long for the Meramec and Kaskaskia, and 30 m wide by 1,100 m long for the Big Muddy River. Daily mean discharge data were taken from the gauge station that was nearest to each tributary's confluence with the Mississippi River. The gauge station at Hermann, MO (Gauge No. 06924500) was used for the Missouri River; the gauge station at Eureka, MO (Gauge No. 07019000) was used for the Meramec River; the gauge stations at Venedy, IL (Gauge No. 05594100) and Freeburg, IL (Gauge No. 05594800) were used for the Kaskaskia River; and the gauge station at Murphysboro, IL (Gauge No. 05599490) was used for the Big Muddy River. The least-squares method was used to find the best-fit form of the rating curve equations for each site. The following non-linear, power-regression equation was used:

$$SSC = \alpha Q^{\beta} + \varepsilon \qquad (2)$$

where SSC is predicted in mgL^{-1}, α is the regression coefficient, Q is discharge in cubic feet per second,

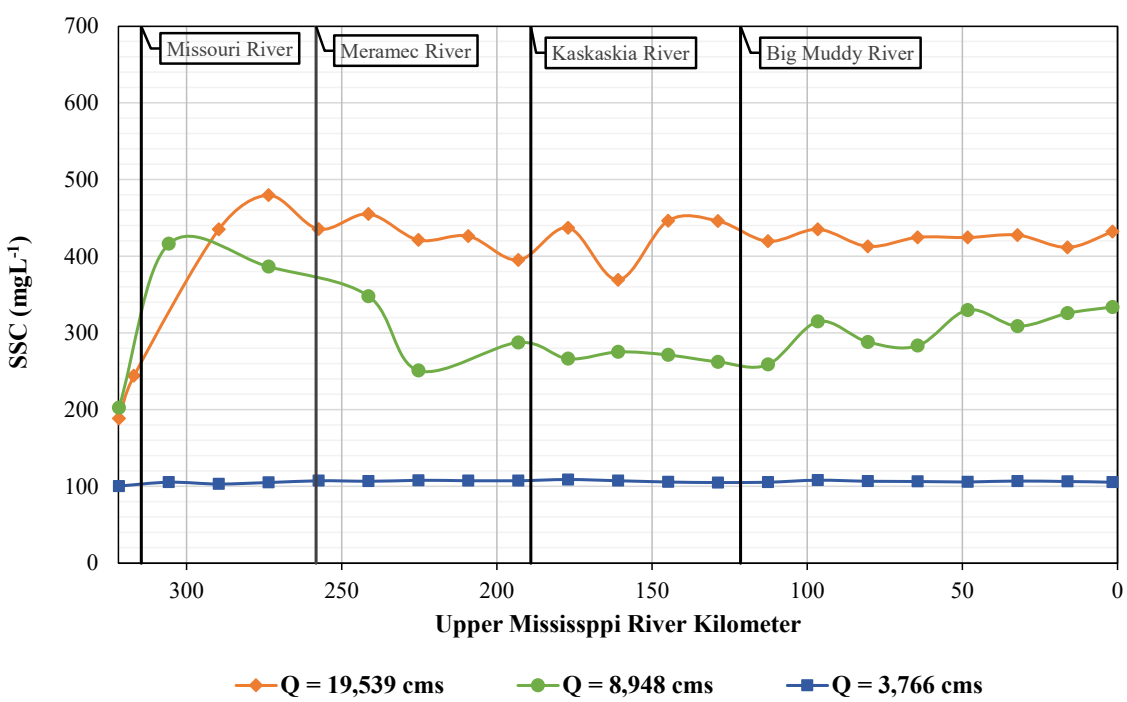

Figure 7. Graph showing SSC along the Middle-Mississippi River (Upper-Mississippi River from River Kilometer 197 to 1) for different flow frequencies.

β is the power term for the discharge, and ε is the constant term.

Observed versus predicted SSC plots for each site, along with the calibrated rating equations, are shown in Figure 8. The Missouri River had an R^2 value of 0.433, the Meramec River had the highest rating curve R^2 value of 0.747, Kaskaskia had an R^2 value of 0.360, and the Big Muddy River had an R^2 value of 0.519. Estimates of sediment yield based on rating-curve calculations will have greater errors than those obtained from direct measurements; however, a sediment rating curve can be valuable in the absence of direct measurements. Asselman (2000) stated that scatter about the rating curve regression line is caused by variations in sediment supply due to seasonal effects, antecedent conditions in the river basin, and differences in sediment availability at the beginning and the ending of a flood, which are not accounted for in rating curves.

Summary and Conclusions

Reflectance-SSC regression models for the

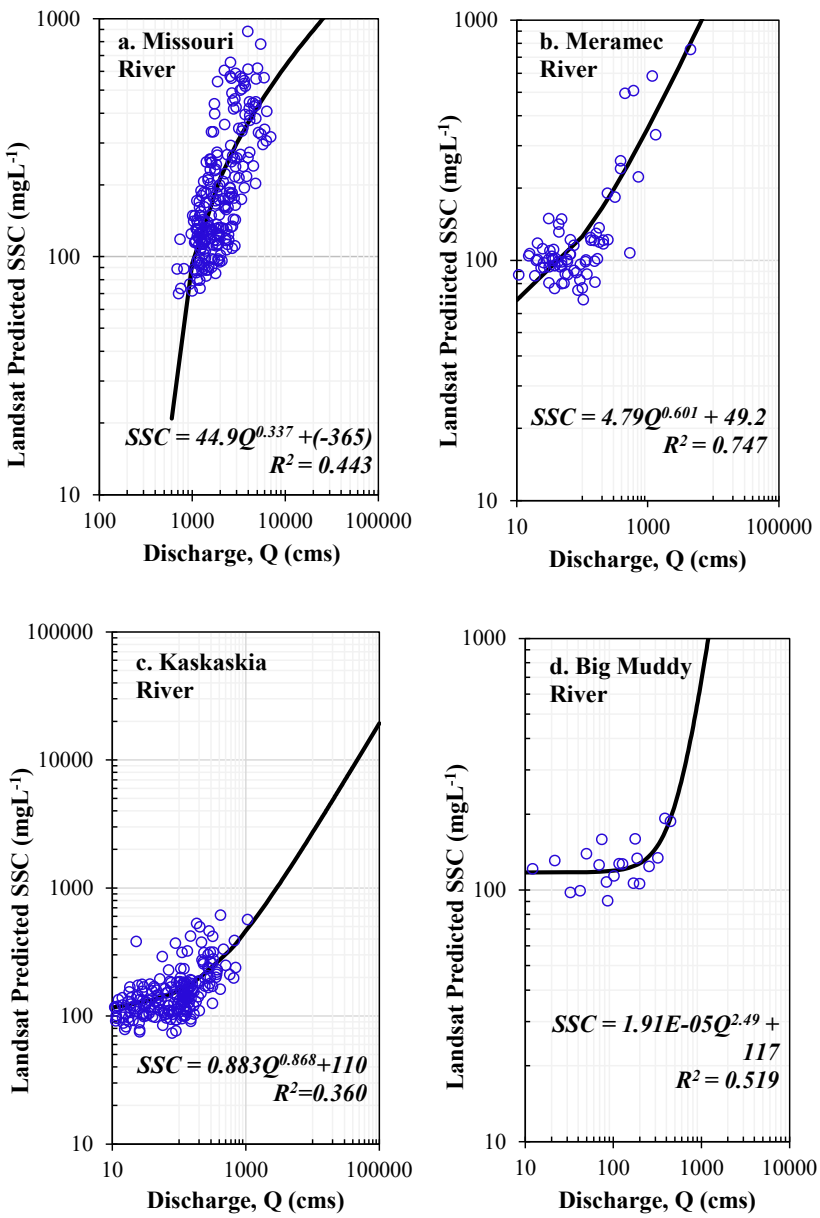

Figure 8. Sediment rating curves obtained from empirical relationship between Landsat predicted SSC and observed discharge for (a) Missouri River, (b) Meramec River, (c) Kaskaskia River, and (d) Big Muddy River.

MMR and the LMOR were developed from Landsat measured surface reflectance and USGS SSC records. The calibrated reflectance-SSC models had validation R^2 values of 0.72, 0.71, and 0.75 for Landsat 8 OLI/TIRS, Landsat 7 ETM+, and Landsat 4-5 TM, respectively. Landsat satellites have been collecting data for 36 years, with a temporal resolution of 16 days. These reflectance-SSC relationships enable researchers to study spatial and temporal trends in SSC for dates of available Landsat data.

Three applications of the reflectance-SSC regression models were demonstrated: 1) mixing at the Mississippi and Missouri River confluence, 2) point-source pollution, and 3) SSC changes along the entire MMR reach for a range of discharges. The following conclusions were made from these analyses:

Analysis of SSC distributions at the Mississippi and Missouri River confluence for September 12, 2016, showed the mixing field extended approximately 161 kilometers downstream of the confluence.

Using the regression models, a point-source pollution location along the MMR was identified with elevated SSC values on dates in five different years. This type of application can be used to identify local areas with consistently elevated SSC that may be causing negative impacts on the MMR.

Longitudinal profile distributions of SSC in the MMR for a range of flow rates revealed that SSC values generally increased with increasing downstream distance and increased with increasing discharges.

The regression models were also used to develop sediment rating curves for the Missouri, Meramec, Kaskaskia, and Big Muddy Rivers. The R^2 values for these rating curves were 0.433, 0.747, 0.360, and 0.519, respectively. The Missouri River is monitored for SSC, but there are gaps in the period of record which can be supplemented with data derived from the sediment rating curves. The remaining three tributaries are unmonitored for SSC and the sediment rating curves can provide an estimate of the sediment load contributions from each tributary to the MMR. In future studies, the sediment rating curves could be used to create a sediment budget for the MMR.

Acknowledgements

Funding for this project came from the USGS Grant G16AP00066 awarded by the Missouri Water Resources Research Center.

Author Bio and Contact Information

Megan Martinez was a graduate research assistant at Saint Louis University from August 2017 to May 2019. She graduated in May 2019 with her Master of Science in Civil Engineering and is currently employed as a Civil Engineer/Site Engineer at M&M Engineering Consultants Limited in Belize. She may be contacted at meganjosephinemartinez@gmail.com or by mail at 3450 Lindell Blvd, St. Louis, Missouri, 63103.

Dr. Amanda L. Cox (corresponding author) is an associate professor of civil engineering and Director of the WATER Institute at Saint Louis University. Her research interests are focused on hydraulic engineering and include hydraulic modeling, sediment transport, hydraulic structures, river engineering and stream restoration, urban drainage, and stormwater erosion. She has a Ph.D. in civil engineering from Colorado State University and is a licensed professional engineer in the states of Missouri and Colorado. She may be contacted at amanda.cox@slu.edu or by mail at 3450 Lindell Blvd, St. Louis, Missouri, 63103.

References

Asselman, N.E.M. 2000. Fitting and interpretation of sediment rating curves. *Journal of Hydrology* 234(3): 228-248.

Dos Santos, B.B., R.B. De Miranda, M.V. Estigoni, J.M. Villela, and F.F. Mauad. 2018. Evaluation of the laser diffraction method for the measurement of suspended sediment concentration in the Mogi-Guacụ reservoir (São Paulo, Brazil). *International Journal of River Basin* 17(1): 89-99.

Doxaran, D., J. Froidefond, and P. Castaing. 2003. Remote-sensing reflectance of turbid sediment-dominated waters. Reduction of sediment type variations and changing illumination conditions effects by use of reflectance ratios. *Applied Optics* 42(15): 2623-2634.

Felix, D., I. Albayrak, and R.M. Boes. 2017. In-situ investigation on real-time suspended sediment measurement techniques: Turbidimetry, acoustic attenuation, laser diffraction (LISST) and vibrating tube densimetry. *International Journal of Sediment Research* 33(1): 3-17.

Gray, J.R. and J.W. Gartner. 2010. Overview of selected

surrogate technologies for high-temporal resolution suspended-sediment monitoring. In: *2nd Joint Sedimentation and Hydrologic Modeling Federal Interagency Conference*, Las Vegas, NV, 27 June - 1 July 2010.

Guerrero, M., N. Ruther, S. Huan, and S. Baranya. 2017. A combined use of acoustic and optical devices to investigate suspended sediment in rivers. *Advances in Water Resources* 102: 1-12.

Islam, M.R., Y. Yamaguchi, and K. Ogawa. 2001. Suspended sediment in the Ganges and Brahmaputra Rivers in Bangladesh: Observation from TM and AVHRR data. *Hydrological Processes* 15: 493-509. Available at: https://onlinelibrary.wiley.com/doi/10.1002/hyp.165. Accessed March 8, 2023.

Landers, M.N. 2012. Fluvial suspended sediment characteristics by high-resolution, surrogate metrics of turbidity, laser-diffraction, acoustic backscatter, and acoustic attenuation. Doctoral Dissertation. Georgia Institute of Technology, Atlanta, Georgia, USA.

Lathrop, Jr., R.G. 1992. Landsat Thematic Mapper monitoring of turbid inland water quality. *Photogrammetric Engineering & Remote Sensing* 58(4): 465-470.

Long, C.M. and T.M. Pavelsky. 2013. Remote sensing of suspended sediment concentration and hydrologic connectivity in a complex wetland environment. *Remote Sensing of Environment* 129: 197-209. Available at: https://doi.org/10.1016/j.rse.2012.10.019. Accessed March 8, 2023.

Mertes, L.A.K., M.O. Smith, and J.B. Adams. 1993. Estimating suspended sediment concentrations in surface waters of the Amazon River wetlands from Landsat images. *Remote Sensing of Environment* 43(3): 281-301. Available at: http://dx.doi.org/10.1016/0034-4257(93)90071-5. Accessed March 8, 2023.

Pereira, L.S.F., L.C. Andes, A.L. Cox, and A. Ghulam. 2018. Measuring suspended-sediment concentration and turbidity in the Middle Mississippi and Lower Missouri Rivers using Landsat data. *Journal of the American Water Resources Association* 54(3): 440-450. Available at: https://dx.doi.org/10.1111/1752-1688.12616. Accessed March 8, 2023.

Peterson, K.T., V. Sagan, P. Sidike, A.L. Cox, and M.J. Martinez. 2018. Suspended sediment concentration estimation from Landsat imagery along the Lower Missouri and Middle Mississippi Rivers using an extreme learning machine. *Remote Sensing* 10(10): 1503. Available at: https://doi.org/10.3390/rs10101503. Accessed March 8, 2023.

Ritchie, J.C., F.R. Schiebe, and J.R. McHenry. 1976. Remote sensing of suspended sediments in surface water. *Photogrammetric Engineering & Remote Sensing* 42(12): 1539-1545.

Ritchie, J.C., C.M. Cooper, and J. Yongqing. 1987. Using Landsat multispectral scanner data to estimate suspended sediments in Moon Lake, Mississippi. *Remote Sensing of Environment* 23: 65-81.

Ritchie, J.C. and C.M. Cooper. 1988. Comparison of measured suspended sediment concentrations with suspended sediment concentrations estimated from Landsat MSS data. *International Journal of Remote Sensing* 9(3): 379-387. Available at: https://dx.doi.org/10.1080/01431168808954861. Accessed March 8, 2023.

Ritchie, J.C., P.V. Zimba, and J.H. Everitt. 2003. Remote sensing techniques to assess water quality. *Photogrammetry and Remote Sensing* 69(6): 695-704.

Topliss, B.J., C.L. Almos, and P.R. Hill. 1990. Algorithms for remote sensing of high concentration, inorganic suspended sediment. *International Journal of Remote Sensing* 11(6): 947-966. Available at: https://dx.doi.org/10.1080/01431169008955069. Accessed March 8, 2023.